Hindawi Publishing Corporation
International Journal of Optics
Volume 2013, Article ID 756402, 9 pages
http://dx.doi.org/10.1155/2013/756402

Research Article

Preparation and Characterization of (Au/n-SnO_2/SiO_2/Si/Al) MIS Device for Optoelectronic Application

Marwa Abdul Muhsien,[1] Evan T. Salem,[2] and Ibrahim R. Agool[1]

[1] *Department of Physics, College of Science, Al Mustansiriyah University, Baghdad, Iraq*
[2] *Laser and Optoelectronic Branch, School of Applied Sciences, University of Technology, Baghdad, Iraq*

Correspondence should be addressed to Marwa Abdul Muhsien; marwa_alganaby@yahoo.com

Received 5 April 2013; Revised 18 September 2013; Accepted 19 September 2013

Academic Editor: Yu S. Kivshar

Copyright © 2013 Marwa Abdul Muhsien et al. This is an open access article distributed under the Creative Commons Attribution License, which permits unrestricted use, distribution, and reproduction in any medium, provided the original work is properly cited.

SnO_2 thin films were prepared by using rapid thermal oxidation (RTO) of Sn at oxidation temperature 873 K and oxidation time 90 sec on semiconductor n-type and p-type silicon substrate. In order to characterize the prepared device, the electrical properties have been measured which revealed that the barrier height is greatly depended on interfacial layer thickness (SiO_2). The value of peak response (n-SnO_2/SiO_2/n-Si) device was 0.16 A/W which is greater than that of (n-SnO_2/SiO_2/p-Si) device whose value was 0.12 A/W, while the rise time was found to be shorter.

1. Introduction

Transparent Conductive Oxides (TCOs) have been extensively studied due to their important technological applications, such as electrochromatic displays, solar cells, and other optoelectronic devices [1]. For these applications, the TCOs should present a combination of high transparency in the visible spectral range and low electrical resistivity. An example of these oxides is the tin oxide (SnO_2) that shows high transmittance in the visible region and a poor conductivity ($\sigma \sim 10^2$–$10^3\ \Omega^{-1}\ cm^{-1}$) at room temperature (~300 K). Moreover, σ value is unstable during its operation due to the reaction of oxygen vacancies in the SnO_2 lattice with ambient oxygen [2]. SnO_2 layers can be deposited using various methods: sputtering [3], pulsed excimer laser ablation deposition (PLAD) [4], chemical vapour deposition (CVD) [5, 6], and spray pyrolysis [7–10]. Tin oxide thin films are n-type semiconductors with a direct optical band gap of about 3.87–4.3 eV [11–14]. Further, its refractive index lies in between 1.9 and 2.0 and hence it can be used as an antireflection (AR) coating. Thermal oxidation is a chemical process, where silicon dioxide (SiO_2) is grown in an ambient with elevated temperatures. A simple form of thermal oxidation even takes place at room temperature, if silicon is exposed to an oxygen or air ambient. There, a thin native oxide layer with (0.5–1 nm) will form on the surface rapidly. After that, the growth slows down and effectively stops after a few hours with a final thickness in the order of (1-2 nm), because the oxygen atoms have too small energy at room temperature to diffuse through the already formed oxide layer.

The reports on the physical properties of other oxide films prepared by thermal oxidation of metallic films revealed a strong dependence of these properties on the heating rate during oxidation process [15]. The desired characteristics and requirements of the fabricated oxide can be mainly influenced by the used oxidant species. For a chosen oxidant species the oxide growth rate usually is controlled by the temperature and time of oxidation. Heterojunction device consisting of a wide band gap semiconductor (usually an oxide semiconductor) mated to a much narrower band gap (active) semiconductor have gained considerable prominence during the past few years. The performance of these devices is strongly controlled by the presence of a thin interfacial insulator layer [11]. Different MIS device structures has been obtained in the last ten years using variable semiconductors as a device substrate. Figure 1 show the metal-insulator-semiconductor structure, since the Si represents semiconductor, the SiO_2 thin layer represents the insulator and the reduction of SnO_2 will produce the metal. A high resistance at the SnO_2-Si interface is attributed to the presence of a semi-insulating interface

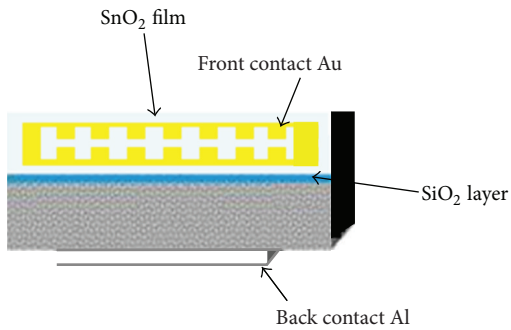

Figure 1: Schematic diagram of the fabricated MIS device.

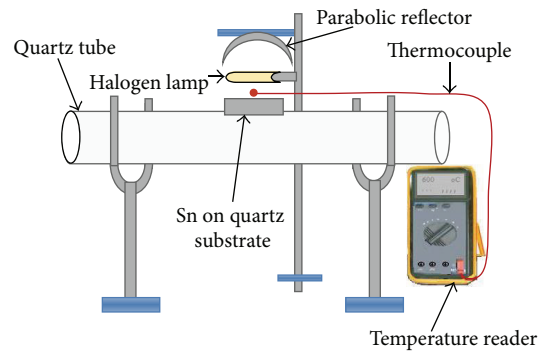

Figure 2: Rapid photothermal oxidation (R.T.O) setup.

layer existing at least in the silicon part as SiO_2 layer, which plays an important role in determining the device efficiency, that is, enhancing the photovoltaic characteristics [16]. It is quite obvious that under processing conditions reduction of SnO_2 is likely to occur by Si; that is, [17]

$$SnO_2 + Si \longrightarrow SiO_2 + Sn. \quad (1)$$

Heterojunction devices have drawn a great attention in recent years mainly due to their use in optoelectronic field [18]. The heterojunction detector is one of the most important junctions because of the wide available technique that can be used to fabricate it, beside the wide range of radiation that could be detected by using this device [19–21]. Current Transport Mechanism of such Heterojunction could be explained according to the diffusion model, the emission model, and the recombination model [22–24], where the relation between J and V is represented by

$$J \propto \exp\left(\frac{qV}{\eta kT}\right), \quad (2)$$

where q/kT is the reciprocal of volt equivalent of temperature and η is the diode factor. The idea of it detected ability depended on the developing of internal voltage within the depletion layer which used to separate the electron-hole pair resulting from the absorption of the light energy incident on the device surface [25]. This mechanism take a specific time dependant on the device characteristic and on the preparation condition; this beside other parameters greatly affected the response time of the detector [26, 27]. This is one of the most important parameters as it can limit the number of applications that a given detector can be used in. Several conventional quantities are often used to describe the characteristics of a given detector; these quantities include: responsivity, spectral response, detectivity and D^*, quantum efficiency linearity, and response time, which is define as the time required for the detector voltage to increase from 10% to 90% from its final value and can be given by the following equation [26, 27]:

$$t_r = \left[t_c^2 + (R_D C)^2\right]^{1/2}, \quad (3)$$

where $R_D = R_S + R_L$ and $C = C_s + C_d$.

Here, t_c = charge collection time, R_s = series resistance, R_L = load resistance, and C_s = capacitance results because of electrical contact. The time constant is greatly affected by carrier diffusion time, carrier drifts time from depletion region, and depletion region capacitance. The aim of this work is to measure the rise time of $SnO_2/SiO_2/Si$ heterojunction device and then estimate the detector response time if the device could be used as a VIS-NIR photodetector and then measure the most importing detector parameters for the optimum one.

2. Experimental Work

N-type and p-type single crystal silicon (111) substrates were used in this work, each of $1 \times 1\,cm^2$ area, of (1.5–4) Ω·cm resistivities were prepared using a wire-cut machine. The silicon substrates were etched with CP4 solution consisting of (HNO_3, and CH_3COOH, HF) of ratios (3 : 3 : 5) to remove oxides. They were then cleaned by alcohol and ultrasonic machine (Cerry PUL 125 device) for 15 minutes then they were cleaned by water and ultrasonic waves for another 15 minutes. High purity of tin (Sn) thin film was deposited on silicon substrate using thermal evaporation technique at room temperature under vacuum pressure of 10^{-6} Torr. SnO_2 film was obtained with aid of rapid photothermal oxidation system with halogen lamp as oxidation source. The oxidation condition used to form SnO_2 film was 600°C/90 s. Figure 2 shows the system used to prepare the oxide film, where a quartz tube of 3 cm diameter with two open ends was used to ensure the flowing of air through it. The source of dry oxygen was used. 650 W halogen lamps were used to provide light and heat radiation and a variable power supply to control the output power. A k-type thermocouple was used to monitor samples temperature. The silicon sample was used as substrate for TCO's/Si heterojunction. Ohmic contacts were fabricated by evaporating 99.999 purity aluminum wires for back contact and 99.999 pure gold were used as front contact through special mask using Edwards coating system.

Measurements of $SnO_2/SiO_2/Si$ Heterojunction Devices. These measurements include the rise time and time constant of the detector is measured by using (LED) with wavelength (820 nm) and the output signal is obtained using a storage

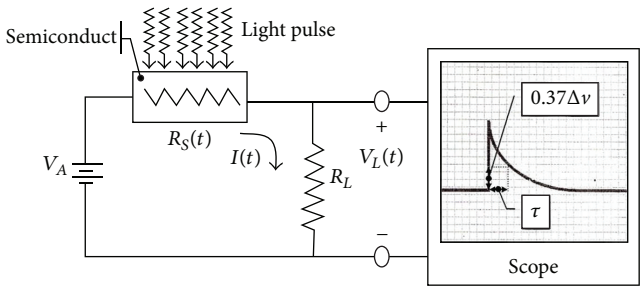

FIGURE 3: Carrier life time setup.

scope type (8300-DCS) (programmable digital Scope) with speed (100 MHz) from (Kenwood company). The response time is given by the following relation [28]:

$$t_s = \frac{t_r}{2.2}, \tag{4}$$

where t_r = rise time.

Carrier life time when the semiconductor is illuminated with photons of sufficient energy, due to the generated additional carriers, the conductivity of the semiconductor increases (resistivity will decrease). The Photoconductive property of semiconductors can be used to determine the excess minority carriers lifetime. The experimental setup is schematically illustrated in Figure 3. The semiconductor sample is chosen to be a bar-shaped with a length of L and a crosssection of A. R_S is the sample resistance, R_L is the load resistance, V_A is a dc voltage, τ is the excess minority carriers life time, and V_L is the load or output voltage. R_S and therefore I and V_L are time dependent parameters.

The measurements also include the electrical characteristics and the detector parameters such as spectral and responsivity were performed using a double-beam UIR-210A spectrophotometer operating within the range (200–1000) nm of wavelengths, while the current measurements were performed using a 8010 DMM Fluke digital multimeter. The spectral responsivity was determined using the following equation [29]:

$$R_\lambda = \frac{I_{\text{ph}}}{P_i}\left(\frac{\text{A}}{\text{W}}\right), \tag{5}$$

where I_{ph} is the measured photocurrent and P_i is the incident optical power.

The detector para-meter include Responsivity, Specific Detectivity (D^*). The specific detectivity was determined using the following equation:

$$D_\lambda^* = \frac{R_\lambda}{I_n}\sqrt{A\Delta f}\left(\text{cm}\cdot\text{Hz}^{1/2}\cdot\text{W}^{-1}\right), \tag{6}$$

where Δf is the noise-band width and I_n is the noise current given by [30]

$$I_n = \sqrt{2qI_d}, \tag{7}$$

where I_d is the dark current.

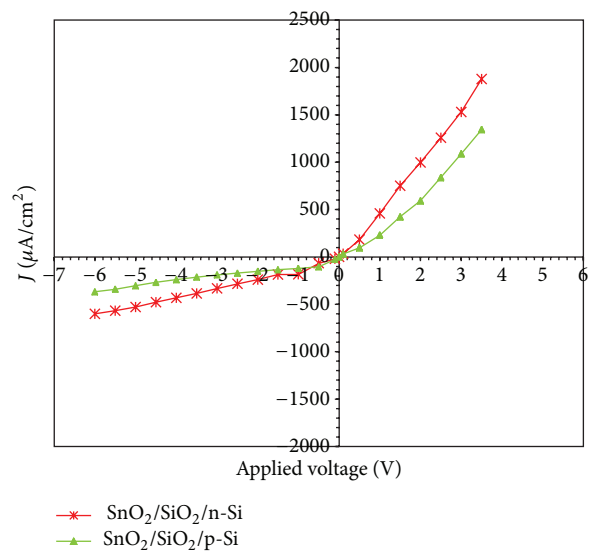

FIGURE 4: J-V characteristic under forward and reverse bias for both MIS devices.

Quantum Efficiency (η). The value of quantum efficiency was estimated using the following equation [31]:

$$\eta = 1.24\frac{\mathscr{K}_\lambda}{\lambda}. \tag{8}$$

3. Results and Discussion

3.1. Electrical Measurements of Constructed Device. The results of the (J-V) measurements at forward and reverse bais in dark for (n-SnO_2/SiO_2/n-Si) and (n-SnO_2/SiO_2/p-Si) devices prepared at optimum conditions are shown in Figure 4. These characteristics are very important to describe the device performance and all device parameters depending on it. The (J-V) characteristics were given for two devices at optimum conditions under reverse bias. It is clear that the curve contains two regions. The first is the generate where the reverse current is slightly increased with the applied voltage and this tends to generation of electron-hole pairs at low bias. In the second region, a significant increase in the reverse bias can be recognized. In this case, the current resulted from the diffusion of minority carriers through the junction. From the obtained result it is clear that the current produced by (n-SnO_2/SiO_2/p-Si) is less than that obtained from the (n-SnO_2/SiO_2/n-Si) which is related to the large junction resistant which reduces the leakage current. The enhancement in the reverse current is related to enhancement in the junction structure, which results in reducing the number of defects at semiconductor-insulator-semiconductor interfaces of the two junctions. These defects result from the strain due to crystal structure, lattice parameter, and probably thermal expansion mismatch. In the forward bias, the forward voltage results in reducing the height of the potential barrier; therefore, majority carriers are able to cross the potential barrier much easier than at zero bias, so that the diffusion current becomes greater

than the drift current. The results are that Figure 4 gives the J-V characteristics behavior of the (n-SnO_2/SiO_2/n-Si) and (n-SnO_2/SiO_2/p-Si) device in the forward bias. Two regions are recognized; the first one represents recombination current; the first current established when the concentration of the generated carrier is larger than the intrinsic carrier concentration (n_i); that is, ($n * p > n_i^2$), which lead to recombination process for mass low applicable. The second region at high voltage represented the diffusion or bending region which depended on serried resistance and in (MIS) case represented the tunneling region. From the comparison between the results obtained for both devices prepared at optimum conditions, it is recognized that the values of the current improved for (n-SnO_2/SiO_2/n-Si) due to decrease in the resistivity for n-type silicon that results in an increase in the electron concentration. This causes a decrease in the hole concentration and thus a reduction in I_s and can be attributed to the increase in the thickness of the SiO_2 layer for (n-SnO_2/SiO_2/n-Si) device [32]. The ideality factor of both devices was estimated at the optimum conditions using (9) and it has been found to be 1.6 and 1.4, respectively. These values refer to good rectification properties for both prepared devices. The large value of n suggests that in this voltage region, the recombination in these devices occurs primarily in the junction depletion region and at the junction interface. In this device the interfacial layer is taken to be a wide gap insulator (SiO_2) which acts as a tunneling barrier to the transport of carrier from one side to the other. As the insulator thickness is increased, the tunneling probability decreases exponentially. Cells without a thin interfacial layer are much less efficient than those with an interfacial layer [33]. Consider

$$n = \frac{q}{kT} \cdot \frac{\Delta V}{\ln\left(J/J_s\right)}, \tag{9}$$

where kT/q is the activation energy and J_s is the saturation current density.

3.2. B-Photovoltaic Measurements of (n-SnO_2/SiO_2/n-Si) and (n-SnO_2/SiO_2/p-Si) Devices. These measurements represent the most important results since they describe the performance of the device and it includes the following measurements.

3.2.1. Current-Voltage Characteristics under Illumination. Figures 5(a) and 5(b) exhibit the photoelectric behavior of the two devices under illumination condition. It is understood that photoelectric effect results from light-induced electron-hole generation at the device and particularly at the depilation region of the n-type and p-type silicon. Under external reverse bias, depletion region of the device extends and as a result, more incident photons will contribute to the electron-hole pairs generation that takes place in the depletion region. The internal electric filed in the depletion region causes the electron-hole pairs to separate from each other and this bias becomes large with the applied external bias. From Figure 5, we can see the increase in the photo-current with increasing incident light intensity, where the large intensity refers to a great number of incident photons and hence large number of separated electron-hole pairs.

3.2.2. Short-Circuit Current and Open-Circuit Voltage. Figures 6 and 7 show the relation between short-circuit current (I_{sc}) and open-circuit voltage (V_{oc}) with the incident photon power of the halogen lamp for both devices. From the obtained result we can recognize the linear relation between (I_{sc}) and V_{oc} with the incident photo power to reach a maximum value beyond which both values for the two devices tend to saturate and become constant. This occurs due to the total separation of the photo-generated electron-hole pairs. A large difference in the obtained results value can be obviously found comparing it. The higher result obtained for n-SnO_2/SiO_2/n-Si device related to the increase in the depletion layer width by adding the interfacial oxide thickness (SiO_2) which means large area for electron-hole pairs separation and hence large photo-current. Open-circuit voltage (V_{oc}) depends on the photo current as given in the following equation and also on the interfacial oxide thickness (SiO_2) [32]:

$$V_{oc} = \frac{KT}{q} \ln\left(\frac{I_{ph}}{I_0} + 1\right). \tag{10}$$

The results also show that the short-circuit current and open-circuit voltage saturate at high power density since the electric field is strong enough to separate any generated pair for a given incident power. For both cases the linear behavior of V_{oc} versus incident power refers to good linearity of the prepared device to work as a detector or solar cell.

3.2.3. Minority Carrier Life Time. Figures 8(a) and 8(b) show the obtained open-circuit voltage decay pulse for devices prepared at optimum conditions the obtained pulse could be divide in to two special regions, the first one is the intermediate injunction region at which the minority carrier concentration in the substrate is larger than that at thermal equilibrium and at the same time less than majority carrier concentration at thermal equilibrium, as a result a Quasi-Fermi level is directly related to the open-circuit voltage as in the following equation [34]:

$$qV_{oc} = E_{fn} - E_{fp} = k_B T \ln\left(\frac{n_p\ p_n}{n_i^2}\right). \tag{11}$$

As a result of this the recombination process takes place to replace the crystal to the thermal equilibrium position. The second region represent the low injunction case at which the minority carrier concentration is less than its concentration at equilibrium, in this case the Fermi level is close to zero, the mass action low could be applicator correctly, that is, $n * p = n_i^2$. Minority carrier life time for (n-SnO_2/SiO_2/n-Si) and (n-SnO_2/SiO_2/p-Si) was found to be (61.8 μsec) and (53 μsec) receptivity and was tabulated in Table 1. The diffusion depth lengths for both devices found to be ($\ell_h = 2{*}10^{-2}$ cm) and ($\ell_e = 4{*}10^{-2}$ cm) receptivity due to the mobility of electron were larger than the mobility of hole.

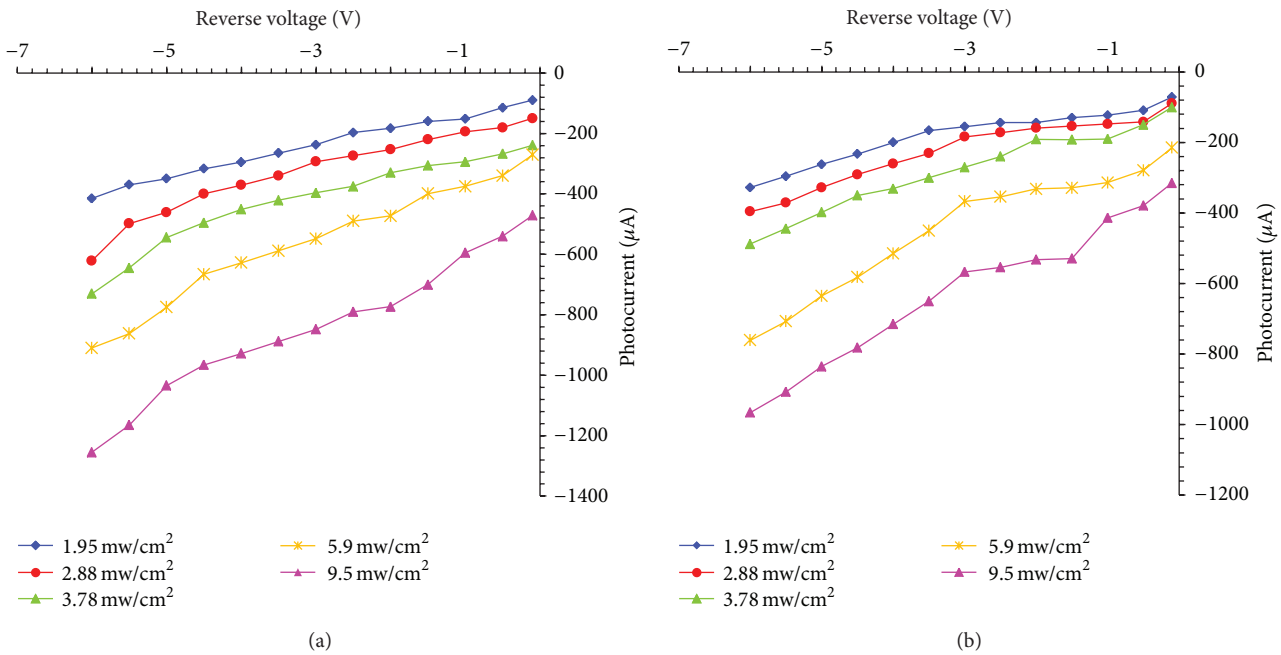

Figure 5: Photo-urrent as a function reveres voltage. (a) (n-SnO_2/SiO_2/n-Si) MIS device, (b) (n-SnO_2/SiO_2/p-Si) MIS device.

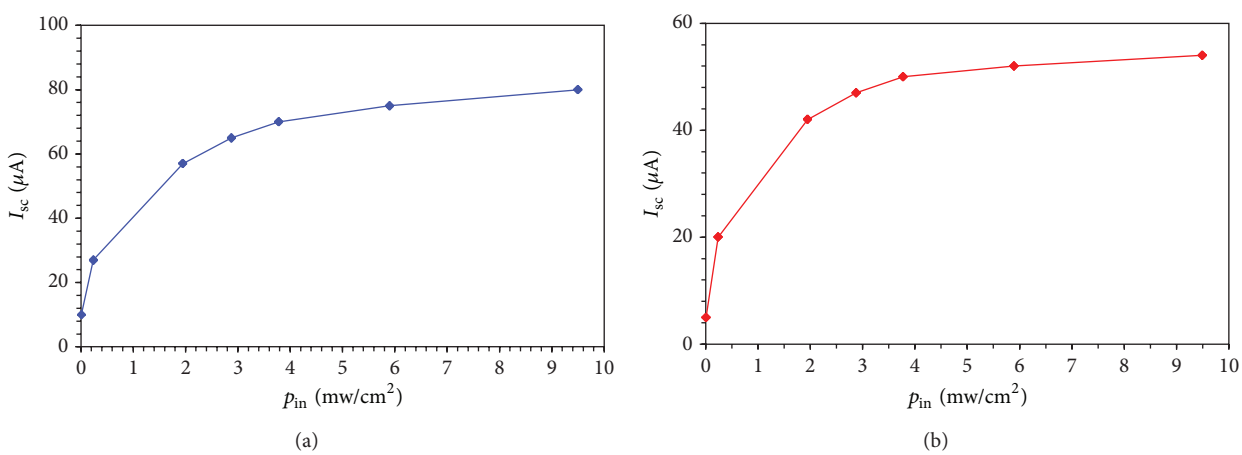

Figure 6: Short-circuit current as a function of the incident photo energy. (a) (n-SnO_2/SiO_2/n-Si) device, (b) (n-SnO_2/SiO_2/p-Si) device.

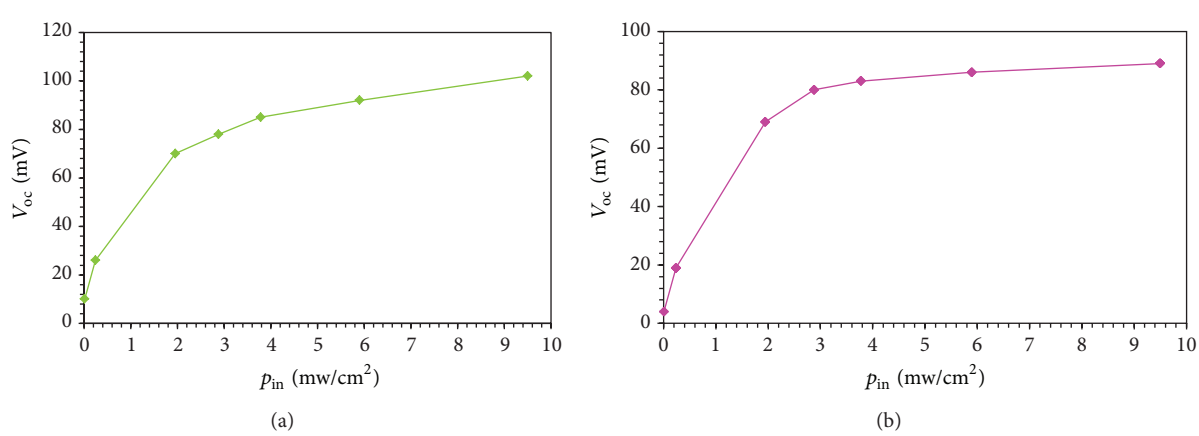

Figure 7: Open circuit voltage as a function of the incident photoenergy. (a) (n-SnO_2/SiO_2/n-Si) device, (b) (n-SnO_2/SiO_2/p-Si) device.

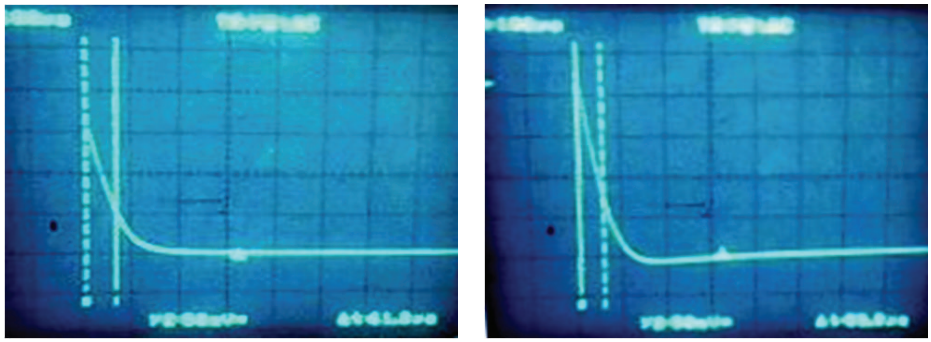

(a) (b)

Figure 8: Carrier life time. (a) (n-SnO_2/n-Si) device, (b) (n-SnO_2/p-Si) MIS device.

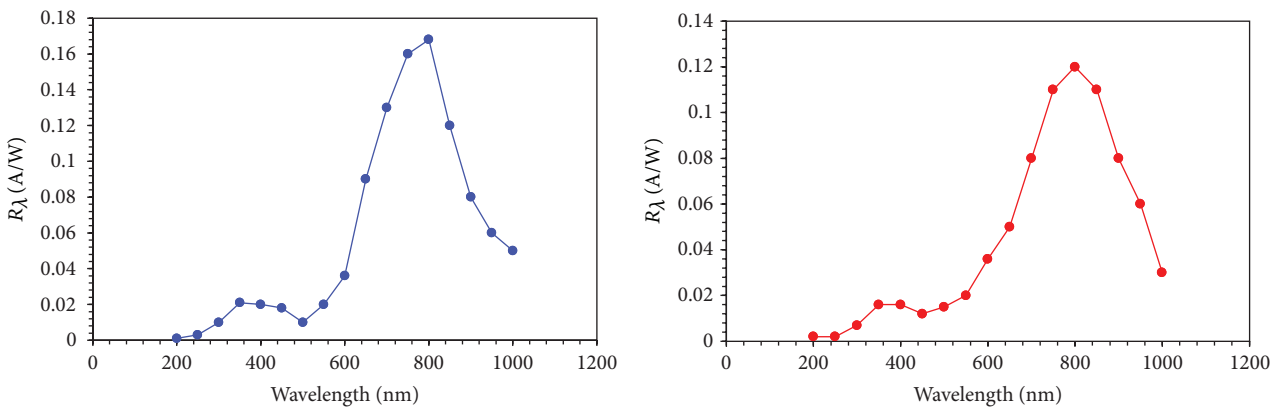

(a) (b)

Figure 9: The spectral responsivity as a function of the incident wavelength. (a) (n-SnO_2/n-Si) device, (b) (n- SnO_2/p-Si) MIS device.

Table 1: The obtained results from the minority carrier life time.

Device type	ℓ_e ℓ_h (cm)	τ_e τ_h (μsec)
n-SnO_2/SiO_2/n-Si	$2 * 10^{-2}$	61.8
n-SnO_2/SiO_2/p-Si	$4 * 10^{-2}$	53

3.3. Measurements of Detector Parameters

3.3.1. Spectral Responsivity. The spectral responsivity represents the ratio between the output generated current to the incident power and it is very important because it specifies the performance range of detector. Figure 9 gives the responsivity as a function of wavelength for both devices prepared at optimum conditions. In both devices, we can recognize three different regions on the curve. The first one (short wavelengths) implies a considerable increase in the responsivity and this increase relates to the high absorption coefficient. This leads to lower absorption depth and fast recombination process compared with any other region inside the material and this is called the probability of carrier concentration, which increases with the departure from the surface region, which means raising the responsivity in this region followed by a decrease in responsivity value which is related to the large surface recombination processes. In the second region (700–900 nm), we observe the highest value of the wavelength-dependent responsivity as these wavelengths are absorbed at the active region of the MIS device junction (depletion region) and a long distance equal to the diffusion length of minority carriers. At this region, the generated electron-hole pairs move due to the internal electric field beside the negligible recombination process in this region. The maximum responsivity appears at 800 ± 50 nm despite the fact that this region is far from the cutoff wavelength. In third region, (>850 nm), the incident light is absorbed within the material where the bulk recombination processes take place, so the carrier concentration probability can exist in this case leading to lower responsivity. Because the SnO_2 semiconductor has a wide and direct band gap, it could be used to collect high energy photons. If the SnO_2 only absorbs in UV and therefore acts as a window for sun light, the barrier is isolated at the interface and should therefore reduce surface recombination and result in larger short-circuit photo current. Furthermore, at the same wavelength, the reflectance indices of SnO_2 and Si match so as to make SnO_2 a candidate for antireflection coating; also it could be expected that a thin layer of SiO_2 will form at the interface during process in and this oxide layer can strongly affect device performance. This makes the SIS structure of SnO_2/Si suitable for use as UV detector.

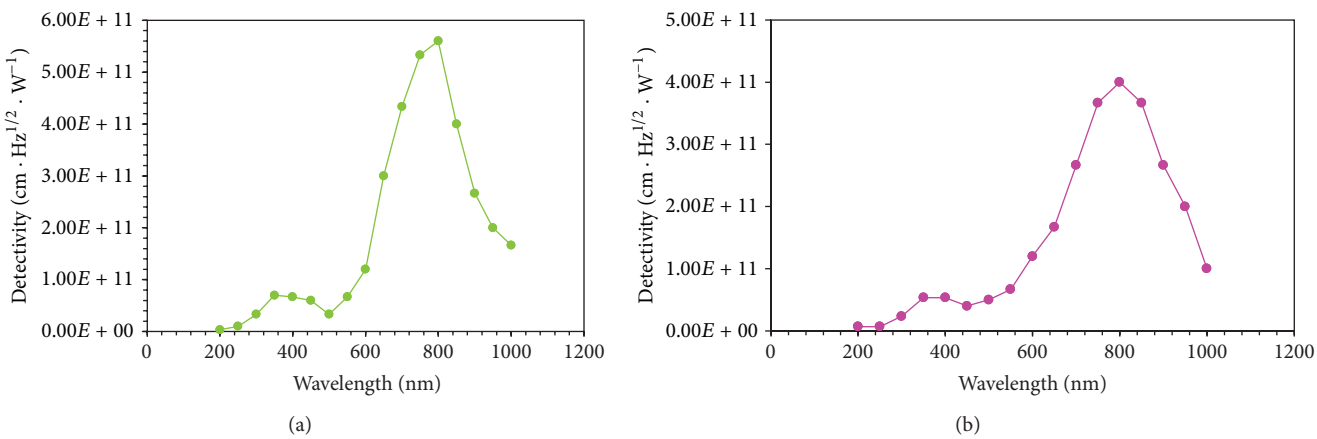

Figure 10: The Quantum efficiency as a function of the incident wavelength. (a) (n-SnO_2/n-Si) device, (b) (n- SnO_2/p-Si) MIS device.

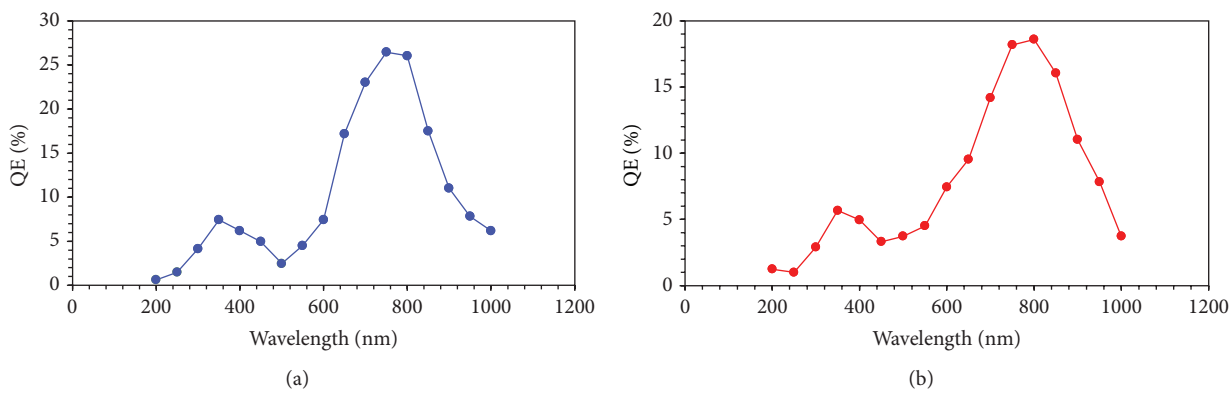

Figure 11: The Specific detectivity as a function of the incident wavelength. (a) (n-SnO_2/n-Si) device, (b) (n-SnO_2/p-Si) MIS device.

3.3.2. Quantum Efficiency. Figure 10 shows the Quantum efficiency of the detector as a function of wavelength. The increase in the photocurrent is attributed to the same reasons of the responsivity. In MIS model, the interfacial layer is taken to be a wide-gap insulator (SiO_2), which acts as a tunneling barrier for carriers transport from one side of the junction to the other. The maximum value of the quantum efficiency in case of (n-SnO_2/SiO_2/n-Si) device is 0.26, while the maximum value of the (n-SnO_2/SiO_2/p-Si) is 0.18. The improvement in the quantum efficiency (η%) is due to increases in thickness of the SiO_2 layer for (n-SnO_2/SiO_2/n-Si) device because of the increase in photo generated current. A decrease in transmission of electrons increasing the interfacial layer thickness leads to reverse current I_o reduction. Thus, the photo-generated current increases.

3.3.3. Specific Detectivity (D^*). The figure of merit of the detectivity D^* is defined as the root mean square (r.m.s.) of the signal to noise ratio (SNR) in 1 Hz band width per unit r.m.s. incident radiant power per square root of the detector area. The specific detectivity versus wavelength is shown in Figure 11 for (n-SnO_2/SiO_2/n-Si) and (n-SnO_2/SiO_2/p-Si) (MIS) devices, directly related to the value of responsivity, so, we can recognize a similarity in the obtained behavior. The most important parameter that specifies the detectivity for a given detector is the noise current (I_n). All the detectors are limited to the minimum radiant power that can be detected in the form of noise, which may arise at the detector itself, in the radiant energy to which the detector responds, or in the electronic circuit following the detector. The most common built-in noises within the detector are white noise, Johnson noise, and thermal noise, which arises from the random motion of the current carriers within any resistance material. Also, the other most important source of noise is the generation-recombination noise that results from the presence of defects acting as trapping centers.

3.3.4. Rise and Response Time. Figures 12(a) and 12(b) represent the obtained rise time pulse of the both MIS devices at wavelength (840) nm.

The idea of the rise time depends on the developing of internal voltage with the depletion region which used to separate the electron-hole pairs resulting from the absorption of the light energy on the device surface. This mechanism takes a specific time depending on the device characteristic.

And since this time constant is greatly affected by carrier diffusion time, carrier drifts time from depletion region, and finally depletion region capacitance, we can understand

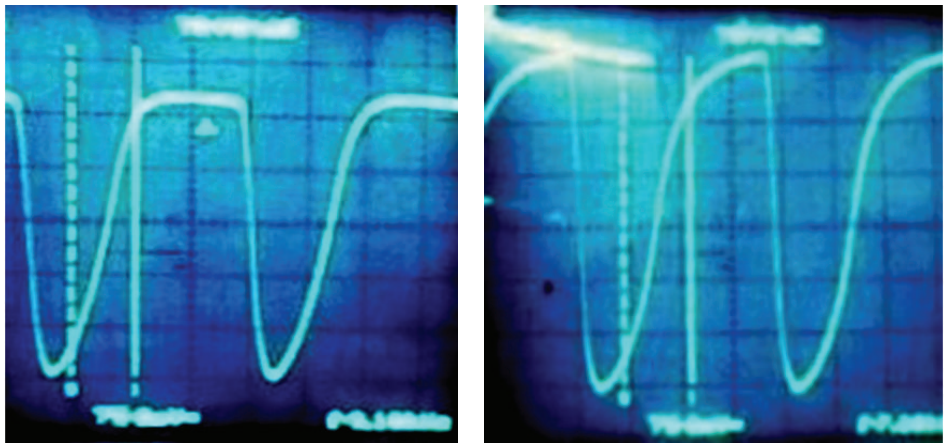

(a) (b)

Figure 12: The response time as a function of the rise time. (a) (n-SnO_2/n-Si) device, (b) (n-SnO_2/p-Si) MIS device.

the enhancement achieved in the case of SnO_2/Si device. Figures 12(a) and 12(b) described the obtained rise time pulse from (n-SnO_2/SiO_2/n-Si) and (n-SnO_2/SiO_2/p-Si), which were found to be 131 μsec and 109 μsec receptivity.

This result gives clear information about the enhancement achieved in the second case; hence, the large reduction appears with the rise time is recognized. This is reflected on the value of the response time achieved which was found to be 59 and 49 μsec for both devices, respectively. The small response time in the second case could be related to the long diffusion of the minority carrier that appeared in the large width of the depletion layer (W) case which is related directly to the diffusion time and mobility of these carriers which reduce the response of the manufactured device.

4. Conclusion

The introduction of an interfacial layer SiO_2 between SnO_2 and Si improves the performance of devices fabricated on n-type and p-type silicon. The electrical and photovoltaic characteristics of (n-SnO_2/SiO_2/n-Si) and (n-SnO_2/SiO_2/p-Si) MIS devices are strongly dependent on the interfacial layer oxide thickness. The ideality factor of both devices was estimated at the optimum conditions using (9) and it has been found to be 1.6 and 1.4, respectively. These values refer to good rectification properties for both prepared devices. The higher result obtained for n-SnO_2/SiO_2/n-Si device related to the increase in the depletion layer width by adding the interfacial oxide thickness (SiO_2) which means large area for electron-hole pairs separation and hence large photo-current. Minority carrier life time for (n-SnO_2/SiO_2/n-Si) and (n-SnO_2/SiO_2/p-Si) were found to be 61.8 μsec and 53 μsec receptivity. The diffusion depth lengths for both devices were found to be ($\ell_h = 2*10^{-2}$ cm) and ($\ell_e = 4*10^{-2}$ cm) receptivity due to the mobility of electron being larger than the mobility of hole. The Spectral Responsivity measurement of (n-SnO_2/SiO_2/n-Si) MIS device is found to be 0.16 A/W while that of (n-SnO_2/SiO_2/p-Si) MIS device is 0.12 A/W. The Rise and Response time measurement of (n-SnO_2/SiO_2/p-Si) MIS device was shorter than that of (n-SnO_2/SiO_2/n-Si) MIS device.

References

[1] R. G. Gordon, "Criteria for choosing transparent conductors," *MRS Bulletin*, vol. 25, no. 8, pp. 52–57, 2000.

[2] K. H. Kim, S. W. Lee, D. W. Shin, and C. G. Park, "Effect of antimony addition on electrical and optical properties of tin oxide film," *Journal of the American Ceramic Society*, vol. 77, no. 4, pp. 915–921, 1994.

[3] T. Karasawa and Y. Miyata, "Electrical and optical properties of indium tin oxide thin films deposited on unheated substrates by d.c. reactive sputtering," *Thin Solid Films*, vol. 223, no. 1, pp. 135–139, 1993.

[4] R. Lal, R. Grover, R. D. Vispute, R. Viswanathan, V. P. Godbole, and S. B. Ogale, "Sensor activity in pulsed laser deposited and ion implanted tin oxide thin films," *Thin Solid Films*, vol. 206, no. 1–2, pp. 88–93, 1991.

[5] J. Jeong, S. P. Choi, K. J. Hong et al., "Atomic scale faceting and its effect on the grain size distribution of SnO_2 thin films during deposition," *Materials Science and Engineering B*, vol. 110, no. 3, pp. 240–242, 2004.

[6] P. Rajaram, Y. C. Goswami, S. Rajagopalan, and V. K. Gupta, "Optical and structural properties of SnO_2 films grown by a low-cost CVD technique," *Materials Letters*, vol. 54, no. 2–3, pp. 158–163, 2002.

[7] I. S. Mulla, V. J. Rao, H. S. Soni, S. Badrinarayanan, and A. P. B. Sinha, "Electron spectroscopic studies on films of SnO_2 and SnO_2: Sb," *Surface and Coatings Technology*, vol. 31, no. 1, pp. 77–88, 1987.

[8] A. P. Rizzato, L. Broussous, C. V. Santilli, S. H. Pulcinelli, and A. F. Craievich, "Structure of SnO_2 alcosols and films prepared by sol-gel dip coating," *Journal of Non-Crystalline Solids*, vol. 284, no. 1–3, pp. 61–67, 2001.

[9] M. Gaidi, *Films minces de SnO_2 dopés au platine ou au palladium et utilisés pour la détection des gaz polluants : analyses in-situ des corrélations entre la réponse electrique et le comportement des agrégats métalliques [Ph.D. thesis]*, l'Institut National Polytechnique, Grenoble, France, 1999.

[10] B. Thangaraju, "Structural and electrical studies on highly conducting spray deposited fluorine and antimony doped SnO_2 thin films from $SnCl_2$ precursor," *Thin Solid Films*, vol. 402, no. 1-2, pp. 71–78, 2002.

[11] D. Hocine, M. S. Belkaïd, and K. lagha, "Influence of interfacial oxide layer thickness on conversion efficiency of $SnO_2/SiO_2/Si(N)$ solar cells," *Revuedes Energies Renouvel Ables*, vol. 11, no. 3, pp. 379–384, 2008.

[12] M. Gökçen, A. Tataroğlu, Ş. Altindal, and İ. Yücedağ, "Effects of gamma radiation stress on electrical characteristics of Au/SnO_2/n-Si (MIS) Diodes," in *Proceedings of the 24th International Physics Congress of Turkish Physical Society*, Malatya, Turkye, 2007.

[13] R. Riveros, E. Romero, and G. Girdillo, "Synthesis and characterization of highly transparent and conductive SnO_2:F and In_2O_3:Sn thin films deposited by spray pyrolysis," *Brazillian Journal of Physics*, vol. 36, no. 3B, 2006.

[14] T. M. Uen, K. F. Huang, M. S. Chen, and Y. S. Gou, "Preparation and characterization of some tin oxide films," *Thin Solid Films*, vol. 158, no. 1, pp. 69–80, 1988.

[15] C. Danţuş, G. G. Rusu, M. Dobromir, and M. Rusu, "Preparation and characterization of CdO thin films obtained by thermal oxidation of evaporated Cd thin films," *Applied Surface Science*, vol. 255, no. 5, pp. 2665–2670, 2008.

[16] D. E. Carlson, "Amorphous silicon solar cells," *IEEE Transactions on Electron Devices*, vol. ED-24, no. 4, pp. 449–453, 1977.

[17] K. Singh and R. Y. Tamakloe, "Power output of Al/SnO_2/n-Si solar cell," *Solar Energy*, vol. 56, no. 4, pp. 343–348, 1996.

[18] M. C. Ko and G. J. Meyer, "Dynamic quenching of porous silicon excited-states," *Chemistry of Materials*, vol. 8, no. 11, pp. 2686–2692, 1996.

[19] J. P. Holfanman, *Introduction to Electronics for Technologestic*, Houghton Mifflin, New York, NY, USA, 1978.

[20] H.-S. Kim, E. C. Zouzounis, and Y.-H. Xie, "Effective method for stress reduction in thick porous silicon films," *Applied Physics Letters*, vol. 80, no. 13, pp. 2287–2289, 2002.

[21] R. Herino, G. Bomchil, K. Barla, C. Bertrand, and J. L. Ginoux, "Porosity and pore size distributions of porous silicon layers," *Journal of the Electrochemical Society*, vol. 134, no. 8, pp. 1994–2000, 1987.

[22] L. T. Canham, "Silicon quantum wire array fabrication by electrochemical and chemical dissolution of wafers," *Applied Physics Letters*, vol. 57, article 1046, no. 10, 1990.

[23] R. JarimaviČiūtė-Žvalionienė, V. Grigaliūnas, S. Tamulevičius, and A. Guobienė, "Fabrication of porous silicon microstructures using electrochemical etching," *Materials Science*, vol. 9, no. 4, 2003.

[24] M. Enachescu, "Light-emitting porous silicon," *Theoretical Study, Journal of Electronic Materials*, 1995.

[25] R. H. Williams, *Metal S/C Interface*, Elumium Press, New York, NY, USA, 1983.

[26] W. Budde, "Optical radiation measurement," in *Physical Detector of the Optical Radiation*, vol. 41, Acadimic press, New York, NY, USA, 1983.

[27] T. S. Clement, P. D. Hale, D. F. Williams et al., "Calibration of sampling scilloscopes with high-speed photodiodes," *IEEE Microwave Theory and Techniques Society*, vol. 54, no. 8, pp. 3173–3181, 2006.

[28] S. M. Sze, *Physics of Semiconductor Devices*, Wiley-Interscience, New York, NY, USA, 1981.

[29] P. Capper and C. T. Elliot, *Infrared Detector and Emitters: Materials and Devices*, Harwood Academic Publishers, NewYork, NY, USA, 2001.

[30] S. Moss, *Hand Book of Semiconductor*, vol. 4, chapter 1, 6B, North-Holland, Amsterdam, The Netherlands, 1986.

[31] R. Vanzeei, *Practical Application of Infrared Techniques*, John Wiley & Sons, New York, NY, USA, 1972.

[32] D. Hocine, M. S. Belkaïd, and K. Lagha, "Influence of interfacial oxide layer thickness on conversion efficiency of $SnO_2/SiO_2/Si(N)$ solar cells," *Revue Des Energies Renouvelables*, vol. 11, no. 3, pp. 379–384, 2008.

[33] A. K. Ghosh, C. Fishman, and T. Feng, "SnO_2/Si solar cells—heterostructure or schottky-barrier or MIS-type device," *Journal of Applied Physics*, vol. 49, no. 6, 1978.

[34] S. M. Sze and K. N. Kwok, *Physics of Semiconductor Devices*, Wiley-Interscience, New York, NY, USA, 3rd edition, 2007.

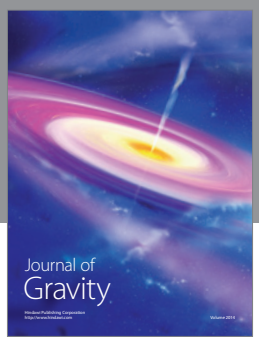

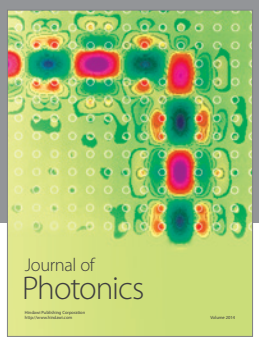

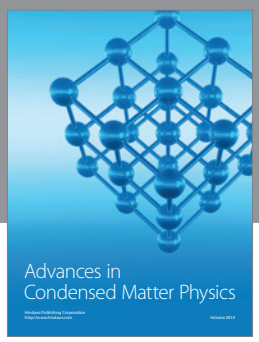

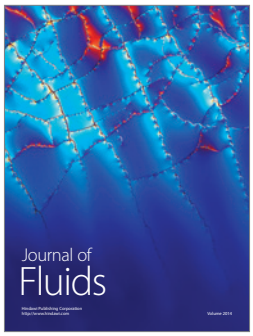

Hindawi

Submit your manuscripts at
http://www.hindawi.com